Numerical Analysis of a Vessel-shaped Offshore Fish Farm

Lin Li[1], Zhiyu Jiang [*2,3], Andreas Vangdal Høiland[1] and Muk Chen Ong[1]

[1]Department of Mechanical and Structural Engineering and Materials Science, University of Stavanger, Stavanger, Norway

[2]Centre for Research-based Innovation on Marine Operations (SFI MOVE), Norwegian University of Science and Technology (NTNU), Trondheim, Norway

[3]Department of Marine Technology, NTNU, Trondheim, Norway

Abstract

The aquaculture industry is aiming to move fish farms from nearshore areas to open seas because of many attractive advantages in the open water. However, one major challenge is to design the structure to withstand the environmental loads due to wind, waves and current. The purpose of this paper is to study a vessel-shaped fish farm concept for open sea applications. The structure includes a vessel-shaped hull, a mooring system and fish cages. The shape of the hull minimizes the wave loads coming from the bow, and the single-point mooring system is connected to the turret at the vessel bow. Such a system allows the whole fish farm to rotate freely about the turret, reduces the environmental loads on the structure and increases the spread area of fish wastes. A basic geometry of the vessel hull was considered and the hydrodynamic properties were obtained from the frequency domain analysis. A mooring system with six mooring lines was designed to avoid possible interactions with the fish cages. Time domain simulations were performed by coupling the hull with the mooring system. A simplified rigid model of the fish cages was considered. The global responses of the system and the mooring line loads were compared under various wave and current conditions. The effects due to misalignment of wave and current directions on the responses were discussed. Finally, the responses using flexible and rigid net models were compared under steady current conditions.

[*] Corresponding author. Email address: zhiyu.jiang@ntnu.no

1 Introduction

There is an increasing demand for seafood production because of the population growth and healthier diet preferences. The amount of captured wild fishes has remained stable in the last few years and the production will remain stagnant or even decline in the future [1]. In contrast, the annual aquaculture production has increased by approximately 10% since 1980, and has played an important role in filling the gap between seafood supply and demand [2]. Most of the fish farms are currently located in sheltered locations, such as fjords and coastal areas. In many countries, such as Norway, the suitable coastal areas for fish farming are almost occupied by operational farms, even in the northern part of the country. Thus, in order to meet the increasing global demand for seafood and to expand the aquaculture industry, new fish farms are forced to move to more exposed open sea locations.

Open cage aquaculture using flexible floating collars is the most practical and popular fish farming technology and has been developed over the last few decades. The whole system often consists of floating collars, nets, bottom weights and a mooring system. The floating collars are normally made of high-density polyethylene (HDPE). They may experience large vertical motions relative to the cross section dimensions, local accelerations, hydroelastic effects and violent wave structure interactions [3]. These effects may introduce fatigue of the flexible collars and cause failure. The large deformation of the net in current is another major issue for the open cage system, and has been studied extensively both numerically and experimentally, e.g. Refs. [4, 5, 6]. Different biofouling organisms accumulated on the net further increase the deformation [7]. The additional drag from biofouling also affects the loads on the mooring system. Modern large fish farms with multiple cages are becoming popular around the world, and the research on the dynamics of multi-cage systems has been brought out based on the methods used for a single cage. The research interests included mooring system analysis, configuration of the cages and flow reductions between successive cages [8, 9]. These researches documented potential failure of the mooring system, as well as excessive deformations of the cages under large wave and current conditions.

There are many benefits of installing fish farms in more exposed seas, including ample space for expansion, tremendous carrying capacity of sea water, reduced conflict with many user groups, lower exposure to human sources of pollution and the potential to reduce some of the negative environmental impacts [1]. However, the traditional open cages using flexible collars and nets are not suitable for exposed locations with harsher environmental conditions, due to problems revealed from previous research. Therefore, novel and robust offshore fish farms should be developed to meet the challenges. This

development has recently been accelerated by the announcement of development licenses in Norway that can be awarded for full scale testing of new concepts which can overcome the current challenges faced by the fish farming industry.

Unlike the flexible floating collars used in current operational farms, several new and potential fish farm concepts with rigid support structures for open seas have been recently proposed by the Norwegian industry. Ocean Farming AS has developed a rigid semi-submersible fish farm [10], which combined technologies from the fields of aquaculture and offshore oil and gas. It comprises fence-like braces, floating elements and a slack mooring system. The nets are tensioned and attached to the braces to avoid deformations in current. Model tests were performed in the ocean basin at SINTEF Ocean [11], and a pilot facility was built in China and is planned to be installed off the coast of central Norway by the second half of 2017 [12].

Aker Solutions AS proposed another rigid semi-submersible fish farm for use in exposed areas. The fish farm comprises a lower and upper pontoon with vertical and diagonal bracing in between [13]. The cage is totally submerged to avoid large wave loads close to the surface, and a submerged air pocket is designed for air supply. The design is aiming to resist extreme waves up to 15 m significant wave height [13]. A numerical study on the global responses of this structure under ocean waves has been carried out [14].

Nordlaks AS proposed a vessel-shaped fish farm with a single-point mooring system [15]. The shape of the hull minimizes the wave loads coming from the bow, and the single-point mooring system is connected to the turret at the vessel bow. Such a system allows the whole fish farm to rotate about the turret and reduce the environmental loads. This mooring system also increases the spread area of fish waste, reducing the probability of fish infections. Figure 1 shows an overview of this concept.

Although many other new concepts have been proposed, to the authors' knowledge, few studies have been published on the hydrodynamic and structural analysis of these concepts. Systematic numerical analyses are essential for the design of any offshore structures to assess the robustness under complicated environmental conditions. The fish farm concepts for exposed seas are novel offshore structures, the state-of-art design code Norwegian Standard NS9415 for conventional fish cages is thus not suitable [16]. Other design codes for offshore oil and gas structures cannot be directly applied to fish farms. Therefore, the lack of specified design code urges the development of research methods for such a novel fish farm structures, and this study presents one example of such development.

This paper addresses numerical analysis of a vessel-shaped fish farm modified based on the design from

Nordlaks [15], see Figure 1. The objective is to present the numerical methods and results of the global response analysis. Reasonable assumptions on the main geometry were made. Due to couplings between different components and nonlinearities from the motions and environmental loads, comprehensive numerical modelling and analysis of the whole fish farm system under combined wind, wave and current conditions are challenging, but important. Therefore, this paper focuses on hydrodynamic and global response analysis. Coupled time-domain analysis are performed to predict the responses under waves and current using a simplified rigid net model. A comparison between the flexible and rigid net models is also made. The description of the fish farm concept, modelling and analysis methods are presented first, followed by discussions of the results. Finally, conclusions and future work are given.

2 Vessel-shaped fish farm concept

2.1 Description of the concept

The concept aims to move from aquaculture pens to aquaculture ships in the open ocean. The vessel-shaped hull which serves as a steel frame for several cages consists of a bow, two main support beams in the longitudinal direction and transverse beams to connect the main support beams. Only the bow and the longitudinal beams are submerged in operational condition, which provide a large opening area for the cages and also reduce the environmental loads on the structure. Steel louse skirts are designed to isolate the fish from the current in the upper layer to reduce the possible influence of sea lice [17].

The whole structure is moored using a single-point mooring system connected to the turret at the vessel bow. Such a system allows the whole fish farm to rotate freely about the turret, reducing the environmental loads and improving water circulation. Another essential advantage of such a mooring system is that the spread area for waste products will be over twenty times larger than ordinary aquaculture pens [17].

In this study, a basic geometry of the vessel hull was considered, and the dimension of the submerged part of the vessel is illustrated in Figure 2. The structure has a total length of 400 m, a breadth of 50 m and a draft of 10 m. Five cone-shaped cages are connected to the hull at 10 m below the mean water surface. Each cage has a 48 m diameter at the top and a depth of 50 m. The cone shape makes the cages less likely to interact with the mooring system than the cylindrical shape.

2.2 Turret and mooring system

A single-point mooring system consisting of six mooring lines with 60 degrees spacing in between is proposed. The mooring lines are connected to the turret located at the bow, see Figure 2. Such a configuration allows the vessel to weathervane passively with minimal stress on the mooring system. Under extreme environmental conditions, the turret can be efficiently disconnected from the vessel, making it possible for the whole fish farm to move to a sheltered area.

Each mooring line is 352 meters long and is composed of the segments listed in Table 1. The chain segments provide adequate restoring forces when the horizontal displacements of the turret are large. The length of the wire ropes is chosen to avoid contact with the seabed. The geometry of the mooring lines does not interfere with the cone-shaped fish cages during motion.

In this paper, a water depth of 120 m is chosen for the numerical analysis, and deeper depths can be used by adjusting the mooring system.

Table 1: Mooring line components

Description	Nominal diameter (mm)	Segment length (m)	Submerged Weight (kN/m)
Anchor	-	-	-
Chain	157	235	4.204
Link	-	1.0	20.0
Wire Rope	130	115	0.686
Link	-	1.0	20.0
Fairlead	-	-	-

3 Hydrodynamic analysis

The hydrodynamic properties of this vessel-shaped fish farm concept were studied in the frequency domain. Linear potential theory was applied, which calculated the added mass, potential damping, first order excitation forces and mean drift forces across relevant wave frequencies [18]. The equations of motions for the rigid body system were solved and the response amplitude operators (RAOs) were computed.

However, the potential flow theory does not include the viscous damping on bluff shapes and sharp edges [19]. As an alternative, Morison elements can be added to include the viscous damping. For this fish farm concept, the two main support beams and the bow are of bluff shapes; therefore, it is important to check the influences of the viscous damping from these components on the global responses. Composite

models with both panel model and Morison elements were defined for comparison, as shown in Table 2.

Table 2: Numerical models for hydrodynamic analysis

Models	Description
M1	Pure panel model, no viscous damping
M2	Panel model + viscous damping on hull (no nets)
M3	Model 2 + simplified rigid nets (Sn = 0.1)
M4	Model 2 + simplified rigid nets (Sn = 0.2)

3.1 Hydrodynamic modelling of the hull and the nets

A first order panel model was generated in the Wadam program [20] for Models 1 to 4. In Model 2, additional viscous damping in terms of Morison elements were added on the hull, including both support beams and the bow. The support beams are rectangular thin plates, and the nondimensional drag coefficient in beam sea direction was chosen as 2.3 for the relevant Reynolds number range ($Re > 10^5$) based on Ref. [21]. The viscous damping on the triangular shaped bow was included using three beams on the edges of the triangle. Equivalent drag coefficients on the beams in vertical and horizontal directions were selected based on two-dimensional coefficients from the DNV recommended practice [22].

For Models 3 and 4, a simplified rigid net system was included. In reality, the nets are flexible structures that deform under wave and current conditions. Strong nonlinearities exist in the hydrodynamic forces on the nets, and nonlinear models are usually required to model the nets [23, 24, 25]. The support structure is relatively large compared to the traditional flexible collars, and the influences of the nets on the hull are expected to be less. Moreover, the nets are located 10 m below the free surface, so the wave forces are greatly reduced.

In the initial phase of the analysis, the nets are modelled as simplified rigid slender elements. This simplification neglects the net deformations, and may overestimate the hydrodynamic forces and viscous effects from the nets. Nevertheless, the simplified rigid model can be used to check the influences of the nets on the global responses of the system. Each cone cage was divided into five horizontal panels and then simplified as five horizontal circular Morison beams. Both horizontal and vertical twines were accounted for in each Morison beam. The drag and lift coefficients C_D^{panel}, C_L^{panel} of the net panel were computed as follows [26, 27]:

$$C_D^{panel} = 0.04 + (-0.04 + 0.33S_n + 6.54{S_n}^2 - 4.88{S_n}^3)cos\theta \tag{1}$$

$$C_L^{panel} = (-0.05S_n + 2.3{S_n}^2 - 1.76{S_n}^3)sin2\theta \tag{2}$$

where S_n is the solidity ratio of the net panel and defined as the ratio of the projected area of the net over the total area. The angle of attack, θ, is defined as the angle between the flow direction and the normal vector to the net panel in the direction of the flow, as shown in Figure 3. When the nets are rigid, the angle for each panel is constant, depending on the conical cage configuration and current direction. The above equations are empirical formula and are limited to S_n ranging from 0.13 to 0.32 [28].

Morison's formula is then applied to the equivalent beams to provide the same hydrodynamic forces on the panels per unit length, see Eq.(3).

$$F = \frac{1}{2}\rho C_D^{beam} D^{beam} \cdot (u + \nu - \dot{x})|u + \nu - \dot{x}| + \rho C_M^{beam} \frac{\pi}{4}(D^{beam})^2 \cdot \ddot{x} \tag{3}$$

where ρ is the fluid density; u is the current velocity; ν is the water particle velocity; $\dot{x}$ and $\ddot{x}$ are the motion velocity and acceleration of the beam element. D^{beam} is the equivalent diameter, and C_D^{beam} is the equivalent drag coefficient. They are obtained using Eq. (4). The same applies for the lift coefficient. In addition, the mass coefficient for each twine, C_M^{twine}, was chosen as 2, and the equivalent mass coefficient of the simplified Morison beam, C_M^{beam}, can be computed based on Eq. (5).

$$C_D^{beam} \cdot D^{beam} = C_D^{panel} \cdot A^{panel} \tag{4}$$

$$C_M^{beam} \cdot (D^{beam})^2 = N \cdot C_M^{twine} \cdot (D^{twine})^2 \tag{5}$$

where A^{panel} is the circumscribed area of the net panel per unit length. D^{twine} is the cross section diameter of the twine. N is the total number of twines represented by the single Morison beam per unit length.

Because the viscous damping effects change significantly with Sn of the nets, two Sn values of 0.1 and 0.2 are assumed for Models 3 and 4, respectively. Common netting materials have solidity ratios in the range of 0.20 to 0.30. Different biofouling organisms will grow on the net cage, further increasing the solidity. However, as mentioned, the simplified rigid Morison elements will overestimate the hydrodynamic forces and viscous effects on the flexible nets. To avoid being over-conservative, relatively low Sn values are chosen in this analysis. Figure 4 illustrates the composite numerical Models 2 and 4 used in the hydrodynamic analysis, where the panel model is shown in blue and the Morison elements are in red.

In order to combine the panel method with the viscous drag of the Morison elements in the frequency

domain, the viscous drag term needs to be linearized. There are several linearization methods, including regular wave linearization and stochastic linearization [29, 30]. In this analysis, stochastic linearization was used, since it takes into account the characteristics of the wave spectrum. The linearized drag coefficient $\bar{C_D}$ for a circular Morison element is given as

$$\bar{C_D} = \frac{1}{2}\rho C_D D\sqrt{\frac{8}{\pi}}\sigma_{|\nu-\dot{x}|} \tag{6}$$

where C_D is the quadratic drag coefficient; D is the diameter of the element; ν is the flow velocity; $\dot{x}$ is the motion velocity of the element; and $\sigma_{|\nu-\dot{x}|}$ is the standard deviation of the flow and the rigid-body motion at the location of the Morison element.

3.2 Eigenvalue analysis

Eigenvalue analysis of the rigid body motions of the fish farm system was also conducted in the frequency domain. The natural modes and the natural periods were obtained by solving Eq. (7).

$$[-\omega^2(\mathbf{M}+\mathbf{A})+\mathbf{K}]\cdot\mathbf{x} = 0 \tag{7}$$

where $\mathbf{x}$ is the natural mode vector corresponding to the eigen frequency ω; $\mathbf{M}$ and $\mathbf{A}$ are the mass and added mass matrices; the added mass with infinite frequency was used. $\mathbf{K}$ is the total restoring matrix including hydrostatic stiffness and linearized mooring stiffness. Table 3 presents the first five natural periods of the system with the dominant rigid body motions for each mode. The sixth mode corresponds to the vessel yaw motion with little restoring from the mooring system, and thus was excluded in the table. From the table, it can be expected that the system may experience resonance motions in the vertical plane with wave periods between 8 to 11 seconds.

Table 3: Undamped natural period of the fish farm system

Mode	Dominant motions	Natural period (s)
1	pitch and heave	8.14
2	roll	8.47
3	heave and pitch	10.60
4	surge	209.32
5	sway	241.72

3.3 Hydrodynamic properties of numerical models

Figure 5 compares the added mass of the structure in surge (A11), roll (A44) and pitch (A55) using different models in Table 2. As expected, the added mass of Models 1 and 2 are the same, since only additional viscous drag on the hull were added to Model 2 compared to the pure panel Model 1. The inclusion of the simplified net cage system increases the total added mass in pitch, especially when Sn is 0.2. This is because the reference point for the added mass is located at the turret centre, where the moment arm for added mass in pitch is large. The increase of added mass in surge and other degrees of freedom is observed to be minor. A peak period (around 7.2 s) with large positive and negative added mass is seen in roll. This is due to the first antisymmetric sloshing mode, e.g., resonant liquid oscillations between the two hull beams. This means that the wave elevations become large at the inner side of the hulls at this peak period. The sloshing period needs to be designed away from the natural frequencies of the structure to avoid resonance. As shown in Table 3, the natural period of the structure in roll is 8.47 s, which is around 1.3 s higher than the period of the sloshing mode.

The main differences between the various hydrodynamic models lie in the damping effects on different parts of the system. Figure 6 compares the potential damping from Model 1 with the linearized viscous damping from Models 2 to 4. A moderate sea state with significant wave height of 4 m and peak period of 10 s is used for the stochastic linearization of viscous damping in all Morison elements in this figure.

It is apparent that the viscous effects from the rigid nets provide more damping than the potential damping from the hull in both heave and roll for most wave periods. Similar observations are seen in surge and pitch. The damping is more than doubled when Sn increases from 0.1 to 0.2. The viscous effects from the hull also contribute to the total damping, but the influences are low compared to those from the nets. Potential damping still dominate the total damping in roll near the first sloshing mode.

Figure 7 shows the wave frequency RAOs in heave and roll using different models. As expected, the RAOs are greatly reduced from Model 1 to Model 2 after implementing viscous damping on the hull. The addition of the rigid nets further decreases the RAOs near the peak periods by more than 20% in heave and 70% in roll, especially when Sn is 0.2. Several peaks can be observed in the heave motion, which indicate couplings between heave, roll and pitch motions. The highest peak of RAO in roll corresponds to the roll natural period, while the second peak around 7 s corresponds to the previously mentioned sloshing mode.

The comparison of hydrodynamic properties indicates the importance of the viscous effects on the hull and the net elements. The solidity ratio of the nets also influences the behaviour of the whole structure

significantly. Therefore, these factors need to be considered in the global response analysis to evaluate the behaviour of the structure under complicated environmental conditions.

4 Time-domain analysis with a simplified rigid net model

The global response analysis can be carried out using both frequency-domain (FD) and time-domain (TD) methods. FD method linearizes the coupled system and provide efficient solutions. However, for complicated coupled fish farm systems, FD method will introduce large errors due to the use of the approximated linear model for the fish farm structures [14]. Therefore, time-domain coupled analysis was applied in this study.

4.1 Coupled model of the system

The fish farm system was modelled using the coupled SIMO-Riflex computer program [31, 32]. SIMO models the rigid body hydrodynamics of the hull structure and Riflex models flexible elements for mooring lines using finite element methods. The linear hydrodynamic properties of the hull structure were imported from the panel method results, and the slow drift forces were computed from the mean drift coefficients based on Newman's approximation [33]. The radiation wave forces were transformed in terms of retardation functions to be used in the TD analysis.

For the mooring system, dynamics due to line motions were considered in the TD by implementing added mass and drag coefficients for the line cross sections. The coupling between the mooring system and the hull structure was also accounted for. Thus, the influence from the mooring line tensions on the motions of the floater was considered and vice versa. These coupling effects were found to be very critical for the estimation of global responses [14].

In the TD analysis, the nets were still modelled as simplified rigid slender elements as described in the hydrodynamic analysis. However, unlike the stochastic linearization used in the frequency domain, the viscous drag forces on the hull and the nets were directly computed in the time domain. The TD simulations were performed for Models 2 to 4 described in Table 2 to compare the influences of different models on the global responses.

Figure 8 illustrates the coupled TD model for Model 4 established in SIMO-Riflex. The global coordinate system (with origin at the turret centre), definition of the wave and current directions and the mooring line numbers are also shown. The directions of the environmental conditions as well as the

motion responses will be given relative to this global coordinate system. The fish cages are represented by horizontal rigid beams. The global responses and mooring line tensions from the TD analysis will be compared for Models 2 to 4 later in this section.

4.2 Environmental conditions

In general, the design of offshore structures requires a complete response analysis under a wide range of wind, wave, and current conditions, including operational and extreme conditions. However, in the present study, the analysis is limited to seven environmental conditions (ECs) with irregular waves and currents, and the wind is excluded.

In Table 4, the first three conditions only include irregular waves which covers mild and moderate wave conditions in the North Sea area, and the "Norway 5" site in Ref. [34] can be referred as a potential site for this fish farm concept. The irregular waves are described by significant wave height (H_s) and spectral peak period (T_p), and the JONSWAP spectrum with peak enhancement factor depending on H_s and T_p are applied in the analysis [22]. Only one wave direction of 180 degrees is applied for these conditions, since the structure is a turret moored weather vane unit. The wave spreading is not considered. The wave and current directions are represented by Dir_w and Dir_c in Table 4.

Table 4: Environmental conditions for time-domain simulations

EC No.	H_s (m)	T_p (s)	U_c (m/s)	Dir_w (deg)	Dir_c (deg)
EC1	2	6	0	180	–
EC2	4	10	0	180	–
EC3	5	12	0	180	–
EC4	5	12	0.25	180	180
EC5	5	12	0.5	180	180
EC6	5	12	0.5	180	135
EC7	5	12	0.5	180	90

In addition to waves, current is also critical for such a fish farm system. The nets may experience larger current loads than wave loads because of the large submergence. Thus, two current speeds (U_c) of 0.25 m/s and 0.5 m/s are added to the highest sea state and are defined as EC4 and EC5, respectively. Uniform current profile over the depth is assumed, and the waves and currents are collinear. In reality, waves and currents may approach the vessel from different directions. The motions of the structure as well as the tensions in the mooring lines will be influenced by the misalignment between the environments [35]. In principle, the misalignment angle between the waves and currents needs to be selected based on

site specific data. In this paper, two representative misalignment conditions using the largest wave and current speed are considered in EC6 and EC7 for comparison.

In the coupled time domain analysis, for each condition, five 3-hour simulations using different seeds were performed to account for the variability of stochastic waves. The statistical results are based on an average of five seeds.

4.3 Global motion responses

The outputs from time domain simulations are time histories of the total responses including motions and forces. Figure 9 shows time histories of the displacement of the origin in the X direction (surge motion), the pitch of the vessel, and the tension in mooring line 1 under condition EC4 using Models 2 and 4. It can be observed that the pitch motion oscillates mainly with the wave frequency (WF), while the X-displacement and mooring line tension contain both wave frequency (WF) and low frequency (LF) components. The WF components are excited due to linear wave forces, while the LF components are excited by higher order nonlinear forces. It is also observed that the responses are sensitive to the numerical models under the same environmental condition.

For the horizontal motions, a mean drift is generated due to the mean wave and current loads. Figure 10 compares the mean drift of the origin in X- and Y-directions under all conditions, while Figure 11 shows the angle difference between the mean vessel heading and the directions of waves and currents.

For EC1 to EC5, the mean drift only occurs in the X-direction since both waves and currents approach in the head seas. When only waves exist, the mean drifts are not sensitive to the numerical models. This is because the mean wave drift forces on the hull dominate, and the forces on the nets are secondary. However, when currents are included, the mean drifts increase significantly for Models 3 and 4 due to increased mean current force on the nets, in particular for Model 4 when Sn is 0.2. For EC6 and EC7 with misaligned waves and currents, the mean drift in Y direction and yaw angle occur. They increase when the current direction moves towards beam seas.

In Figure 11, the red bars highlight the relative angle between the mean vessel heading and the current direction. The definition of the wave and current directions refers to Figure 8. It can be seen that the vessel tends to align itself more with the currents than with the waves. For example, the relative angle between the vessel and the waves is around 70 degrees at EC7, while the relative angle with current is only 20 degrees. This indicates that the mean current loads are more significant than the mean wave drift forces, and the current dominates the heading of the fish farm structure under the chosen ECs.

Figure 12 compares the wave frequency (WF) and low frequency (LF) components for the horizontal motions. Here, WF components are defined as oscillations with periods between 5 s and 30 s, and LF components are for periods larger than 30 s. Standard deviations (STD) of each component are computed by filtering the whole time series into different frequency ranges. For each EC, the results from Models 2 to 4 are compared. It is obvious that the LF components dominate the horizontal motions for all ECs. The WF components are similar under the same EC using different models, but the LF components reduce significantly after adding the net elements in the model. This is because of the increase in the dynamic damping from the nets. However, as discussed earlier, the use of the rigid net elements overestimates the damping effects. Thus, the dynamic motions may be underestimated by Model 4.

The mean values and standard deviations of WF and LF components for heave, roll and pitch are presented in Figure 13. Unlike the horizontal motions, these motions are dominated by the WF components under all conditions. The mean values for heave and pitch are close to zero for most conditions, but the mean value for roll increases in EC7. This is caused by the mean current forces, which act on the nets with around 20 degrees with respect to the vessel heading, as shown in Figure 11. While the heave and pith motions are not sensitive to the numerical models, the roll motions are more influenced by the addition of damping on the nets in EC7, where the WF components in roll are reduced.

The results presented in Figures 10 to 13 show large motions of the vessel under combined wave and current conditions. The mooring lines in general follow the motions of the turret located in the bow and simultaneously experience dynamic motions due to the dynamic wave and current loads. The deformation of the flexible nets is also expected to be significant. Therefore, it is important to check the relative motions between the mooring lines and the nets, so interactions which may result in the tear and wear of the nets can be avoided. In addition, hydrodynamic interactions between the net cages exist, which will influence the calculation of hydrodynamic forces on the net elements. For example, the current velocities felt by the net elements in the downstream position will be different from the incoming current velocities. The interaction may influence the global motions and tensions in the mooring system, and this will be discussed in Section 5.

4.4 Tensions in the mooring lines

The maximum tension in the considered load cases is observed to be well below the maximum breaking load of the mooring lines. Thus, we use the most probable maximum (MPM) of the mooring line tension in 3 hours as a reference for comparison. The time-domain simulations output time histories of the

mooring line tensions, from which the local maxima between adjacent zero up-crossings are assumed to be independent and are fitted by a 3-parameter Weibull distribution. The MPM corresponds to the peak value of the probability distribution function [22].

Figure 14 compares the maximum tension MPM among six mooring lines for different ECs using Models 2, 3 and 4. It can be observed that for the wave-only cases, the tension MPM decreases after adding the net elements due to increased damping. Current increases the tension MPM significantly for Models 3 and 4. The wave-current misalignment increases the mooring tension for Models 2 and 3, but has less influence on Model 4. This is because the mooring line tensions of Models 2 and 3 are dominated by wave loads, which increase when the vessel heading changes towards the current direction in EC6 and EC7. It is also seen that the largest tension from Models 2 and 3 occurs in EC6 when the relative angle between the currents and waves is 45 degrees.

Figure 15 presents the tension MPM of all six mooring lines for EC5 to EC7 using Model 4. It is observed that when the waves and currents are collinear (EC5), the tensions in lines 2 and 3 are equal to those in lines 6 and 5 because of the symmetry of the mooring layout. The maximum MPM occurs in line 1. However, with increased angle between the waves and currents, the maximum MPM shifts from line 1 to line 6 due to the changing heading of the vessel. For different environmental conditions, the maximum tension MPM occurs at EC7 when the wave and current are 90 degrees misaligned. Therefore, it is important to take into account the misalignment of different environmental loads when designing the mooring system.

Furthermore, Figure 16 compares the mean value, and two times of the standard deviations of WF and LF components for the tension in line 1. In general, the mean tension contributes most to the total tension and it increases dramatically with current speed and the inclusion of the net elements. The LF components decrease from Models 2 to 4 when only waves are present because of the increased damping from the net elements. However, the LF components are similar using three models when current also acts on the structure. The WF components are secondary compared to the LF components, and they increase when the vessel changes heading in EC6 and EC7. The maximum tension in line 1 occurs in EC5 and EC6, while mooring line 6 experiences more tension in EC7.

5 Comparison of the rigid and flexible net models

5.1 Modelling of flexible net and current velocity reduction factor

The time-domain simulations performed in the previous section used the model with simplified rigid nets. In reality, the nets hanging under the vessel hull are flexible structures. A bottom weight is used under each cage to tension the net and maintain the volume of the cages (see Figure 2). Nevertheless, the cages will experience different degrees of deformation depending on the wave and current conditions. The drag and lift forces of the net elements changes with the deformation, and the global responses of the whole system may deviate from the simplified model using non-deformable rigid net cages. Therefore, a numerical model with flexible net elements was also established using the SIMA program.

Unlike the rigid net model, where equivalent horizontal beams were used to represent the net, the cage is divided into 24 net panels circumferentially in the flexible net model. The purpose is to calculate the cage deformation conveniently. Each net panel is then represented by a slender line consisting of bar elements, as shown in Figure 17. Equivalent properties of the twines within the net panel are calculated and applied on the bar elements, including mass, volume and axial stiffness. The detailed properties of the net can refer to Ref. [36]. The hydrodynamic drag and lift coefficients are also calculated based on Eqs. (1) and (2). Under different environmental conditions, the angle of attack, θ, of each bar element (refer to Figure 3) will change due to deformation of the net panels, and the total drag and lift forces will change accordingly.

Furthermore, the current velocity reduction has been taken into account. Due to the loss of momentum when water flows through a net, a continuing reduction of flow velocity occurs in the downstream cages. This is especially important for the present concept where several net cages are positioned in a row parallel to the current direction. The current velocity of the flexible cage is calculated using the engineering approach suggested by Løland [26, 27].

$$u_i = U \cdot r^{i-1} \tag{8}$$

$$r = 1 - 0.46 \cdot C_D \tag{9}$$

where u_i is the local current velocity at the i^{th} net panel facing the flow. r is the current velocity reduction factor behind a net panel. C_D is the drag coefficient on the net panel for a given Sn. Since each cage consists of the front and rear parts, i from 1 to 10 is used for corresponding part of the five conical cages.

5.2 Results and discussions

In this paper, only quasi-static analysis under uniform current conditions has been performed using the flexible net model. Figure 18 shows the deformation of the cages under three different current velocities. It is obvious that the deformation increases significantly with current velocity. The individual cage deformation weakens from cage 1 to cage 5 because of the current velocity reduction, and these reduction effects are dramatic at current larger than 0.5 m/s. For the same reason, deformations of the upstream elements are observed to be larger than those of the downstream elements within one cage.

Figure 19 compares the mooring line tension in line 1 (refer to Figure 8) and the absolute drift motion of the turret centre under various conditions, using flexible and rigid net models. Results with and without current velocity reduction factors are included for both models. The responses are obtained when the coupled system has reached equilibrium under each current velocity.

It is evident that the rigid net model overestimates the responses under strong current conditions. The overestimation is over 30% for both the tension and the drift motions at current velocities larger than 0.8 m/s without reduction factors. The deformation of the flexible nets increases the angle of attack of the net panels (refer to Figure 3), thus reducing the drag forces on the whole fish cage. Nevertheless, this simplified model is still a good approximation for the global responses at current velocities less than 0.5 m/s, and the differences between the rigid and the flexible models are less than 10%. The differences are expected to increase when using higher Sn values.

The results also reveal the importance of the current velocity reduction, which decreases the drag forces on the downstream cages, resulting in lower responses of the whole system. For the flexible model, the average overestimations without reduction factors are about 15% for the tensions and 40% for the drift motions. The influences from velocity reduction on the global responses are more significant than the flexibility of the nets for the present fish farm concept. This can be observed from Figure 19, where the flexible model without reduction factor predicts higher responses than the rigid model with reduction factor for current velocities less than 0.9 m/s. However, the reduction factor applied in this model, see Eq. (9), is only based on studies with planar net panels. The shape and deformations of individual cages were not considered, which may influence this reduction factor. Therefore, extensive studies are required to obtain accurate current velocity reduction factors and to improve the numerical results.

The dynamic analysis with flexible nets under waves or current conditions is out of the scope of this paper. Thus, the dynamic effects of the rigid and flexible nets are not compared. However, it is worth mentioning that the computational efficiency for performing dynamic analysis of flexible nets using the

finite element method is very low. As 3-hour dynamic analyses are normally required in stochastic waves, using the flexible model is very computationally expensive. Therefore, in the initial design phase of a novel fish farm concept, using the simplified rigid net model is efficient for load case screening. For example, the rigid model can be applied to find the most critical environmental conditions, including misaligned directions between current and waves, by performing analysis under a large number of cases. Then, only a limited number of cases under the most critical conditions are required with the flexible model, e.g., for the ultimate limit state design. In addition, by tuning the hydrodynamic coefficients on the rigid nets, it is possible to improve the rigid model and to predict more accurate global responses. The improved rigid model can be further applied to the fatigue limit state design of the global components, e.g. the mooring system. However, the tuning of coefficients requires further comparisons between the rigid and flexible models in dynamic conditions, which will be studied in the future work.

6 Conclusions

This paper presents a numerical investigation on a vessel-shaped floating fish farm. The concept aims to move the traditional aquaculture pens to aquaculture ships in the open ocean. The concept can also increase the spread of waste using a single point mooring system.

Global responses of the vessel and tensions in the mooring lines were computed based on the hydrodynamic properties from the frequency domain. Time-domain simulations with simplified rigid nets were performed and the responses under several wave and current conditions were compared. The inclusion of net elements in the numerical models and the presence of current affect the drift motions of the vessel and tensions in the mooring lines. Under misaligned wave and current conditions, the vessel tends to be more aligned with the current than with the waves, which increases the wave forces on the vessel and its vertical motions. The largest tension occurs when the current and waves are 90 degrees misaligned in this study.

A comparison of the flexible and rigid net models were studied under uniform current conditions. The simplified rigid net model overestimated the global drift motion and mooring line tensions in strong currents compared to the deformable flexible net model. However, the rigid model provided consistent results for current speeds lower than 0.5 m/s, and it can be beneficial for screening analysis under a large number of load cases. More studies should be performed to evaluate the dynamic behaviour of the fish farm with flexible net models. Comparisons of the two models in the dynamic analysis will also be further studied to tune the parameters and improve the simplified rigid model, which can save significant

computational time.

In the numerical modelling and response analysis, assumptions and simplifications were applied. The hydrodynamic properties presented were based on a linear model, and nonlinear effects considering the changing mean positions of the structure under extreme environmental conditions need to be implemented. The hydroelasticity of the hull was not included. The present geometry of the structure and the mooring system was based on an initial design, and optimisation is required. Future work should address the above limitations. However, the numerical method presented in this study is useful for making efficient assessment for offshore fish farms.

ACKNOWLEDGEMENTS

The authors are grateful to Håkon Ådnanes from NSK Ship Design and Dr. Xiaopeng Wu from IKM Ocean Design for valuable discussions. The support from SINTEF Ocean for the SIMA program is also acknowledged.

References

[1] Burnell, G., and Geoff, A, eds, 2009. *New technologies in aquaculture: Improving production efficiency, quality and environmental management.* Elsevier.

[2] Tidwell, J., 2012. *Aquaculture production systems.* John Wiley & Sons.

[3] Li, P., Faltinsen, O. M., and Lugni, C., 2016. "Nonlinear vertical accelerations of a floating torus in regular waves". *Journal of Fluids and Structures,* ***66***, pp. 589–608.

[4] Kristiansen, T., and Faltinsen, O. M., 2012. "Modelling of current loads on aquaculture net cages". *Journal of Fluids and Structures,* ***34***, pp. 218–235.

[5] Moe-Føre, H., Endresen, P. C., Aarsæther, K. G., Jensen, J., Føre, M., Kristiansen, D., Fredheim, A., Lader, P., and Reite, K.-J., 2015. "Structural analysis of aquaculture nets: Comparison and validation of different numerical modeling approaches". *Journal of Offshore Mechanics and Arctic Engineering,* ***137***(4), p. 041201.

[6] Zhao, Y.-P., Li, Y.-C., Dong, G.-H., Gui, F.-K., and Teng, B., 2007. "Numerical simulation of the effects of structure size ratio and mesh type on three-dimensional deformation of the fishing-net gravity cage in current". *Aquacultural Engineering,* ***36***(3), pp. 285–301.

[7] Moe-Føre, H., Lader, P., Lien, E., and Hopperstad, O., 2016. "Structural response of high solidity net cage models in uniform flow". *Journal of Fluids and Structures,* ***65***, pp. 180–195.

[8] Xu, T.-J., Dong, G.-H., Zhao, Y.-P., Li, Y.-C., and Gui, F.-K., 2012. "Numerical investigation of the hydrodynamic behaviors of multiple net cages in waves". *Aquacultural engineering,* ***48***, pp. 6–18.

[9] Turner, A. A., Jeans, T. L., and Reid, G. K., 2016. "Experimental investigation of fish farm hydrodynamics on 1:15 scale model square aquaculture cages". *Journal of Offshore Mechanics and Arctic Engineering,* ***138***(6), p. 061201.

[10] SalMar Group, 2016. Offshore fish farming - a new era! Available at `http://www.salmar.no/en/offshore-fish-farming-a-new-era`. Accessed: 2016-09-07.

[11] MARINTEK, 2016. Offshore salmon fish farming. Available at `http://www.sintef.no/en/projects/offshore-salmon-fish-farming`. Accessed: 2016-09-07.

[12] gCaptain, 2016. Worlds first offshore fish farm rig to be moored off Norway. Available at `http://gcaptain.com/worlds-first-offshore-fish-farm-rig-to-be-moored-off-norway/`. Accessed: 2017-02-02.

[13] Stensvold, T., 2016. Arctic Offshore Farming - Riggeksperter i Aker Solutions lanserer nytt merdkonsept. Available at `http://www.tu.no/artikler/riggeksperter-i-aker-solutions-lanserer-nytt-merdkonsept/346030`. Accessed: 2016-09-07.

[14] Li, L., and Ong, M. C., 2017. "A preliminary study of a rigid semi-submersible fish farm for open seas". In Proceedings of the 36th International Conference on Ocean, Offshore and Arctic Engineering, June 25-30, 2017, Trondheim, Norway.

[15] Nordlaks, 2015. Havfarm. Available at `http://www.nordlaks.no/Om-oss/Havfarm`. Accessed: 2016-09-07.

[16] StandardsNorway, 2009. *NS9415: Marine fish farms: Requirements for design, dimensioning, production, installation and operation.* Standards Norway.

[17] NSK ship design, 2016. NSK - 3417 offshore fish farm. Available at `http://www.nskshipdesign.com/designs/aquaculture/fish-farm/`. Accessed: 2016-09-07.

[18] Lee, C. H., 1995. *WAMIT theory manual*. Department of Ocean Engineering, Massachusetts Institute of Technology, USA.

[19] Faltinsen, O. M., 1990. *Sea Loads on Ships and Ocean Structures*. Cambridge University Press.

[20] DNV, 2008. *Wadam theory manual*.

[21] Tian, X., Ong, M. C., Yang, J., and Myrhaug, D., 2014. "Large-eddy simulation of the flow normal to a flat plate including corner effects at a high reynolds number". *Journal of Fluids and Structures,* ***49***, pp. 149–169.

[22] DNV, 2010. *Recommended Practice DNV-RP-C205, Environmental conditions and enviromental loads*. Det Norske Veritas, Oslo, Norway.

[23] Lader, P. F., and Fredheim, A., 2006. "Dynamic properties of a flexible net sheet in waves and currenta numerical approach". *Aquacultural engineering,* ***35***(3), pp. 228–238.

[24] Lee, C. W., Lee, J., and Park, S., 2015. "Dynamic behavior and deformation analysis of the fish cage system using mass-spring model". *China Ocean Engineering,* ***29***(3), pp. 311–324.

[25] Moe, H., Fredheim, A., and Hopperstad, O., 2010. "Structural analysis of aquaculture net cages in current". *Journal of Fluids and Structures,* ***26***(3), pp. 503–516.

[26] Løland, G., 1991. *Current Force On and Flow Through Fish Farms. Dr. ing dissertation*. Division of Marine Hydrodynamics, the Norwegian Institute of Technology.

[27] Løland, G., 1993. "Current forces on, and water flow through and around, floating fish farms". *Aquaculture International,* ***1***(1), pp. 72–89.

[28] Lader, P. F., and Enerhaug, B., 2005. "Experimental investigation of forces and geometry of a net cage in uniform flow". *IEEE Journal of Oceanic Engineering,* ***30***(1), pp. 79–84.

[29] Wolfram, J., 1999. "On alternative approaches to linearization and morison's equation for wave forces". In Proceedings of the Royal Society of London A: Mathematical, Physical and Engineering Sciences, Vol. 455, pp. 2957–2974.

[30] Shao, Y.-L., You, J., and Glomnes, E. B., 2016. "Stochastic linearization and its application in motion analysis of cylindrical floating structure with bilge boxes". In Proceedings of the 35th International Conference on Ocean, Offshore and Arctic Engineering, June 19-24, 2016, Busan, South Korea.

[31] MARINTEK, 2015. *SIMO - Theory Manual Version 4.6.*

[32] MARINTEK, 2015. *RIFLEX Theory Manual Version 4.6.*

[33] Newman, J. N., 1974. "Second-order, slowly-varying forces on vessels in irregular waves". In International Symposium on the Dynamics of Marine Vehicles and Structures in Waves, University College, London.

[34] Li, L., Gao, Z., and Moan, T., 2015. "Joint distribution of environmental condition at five european offshore sites for design of combined wind and wave energy devices". *Journal of Offshore Mechanics and Arctic Engineering,* ***137***(3), p. 031901.

[35] DNV, 2013. *Offshore Standard DNV-OS-E301, Position mooring.* Det Norske Veritas, Oslo, Norway.

[36] Høiland, A. V., 2017. *Dynamic Analysis of a Vessel-shaped Fish Farm for Open Sea, Master's thesis.* Faculty of Science and Technology, University of Stavanger.

List of Figures

Figure 1: Overview of the vessel-shaped fish farm concept [15].

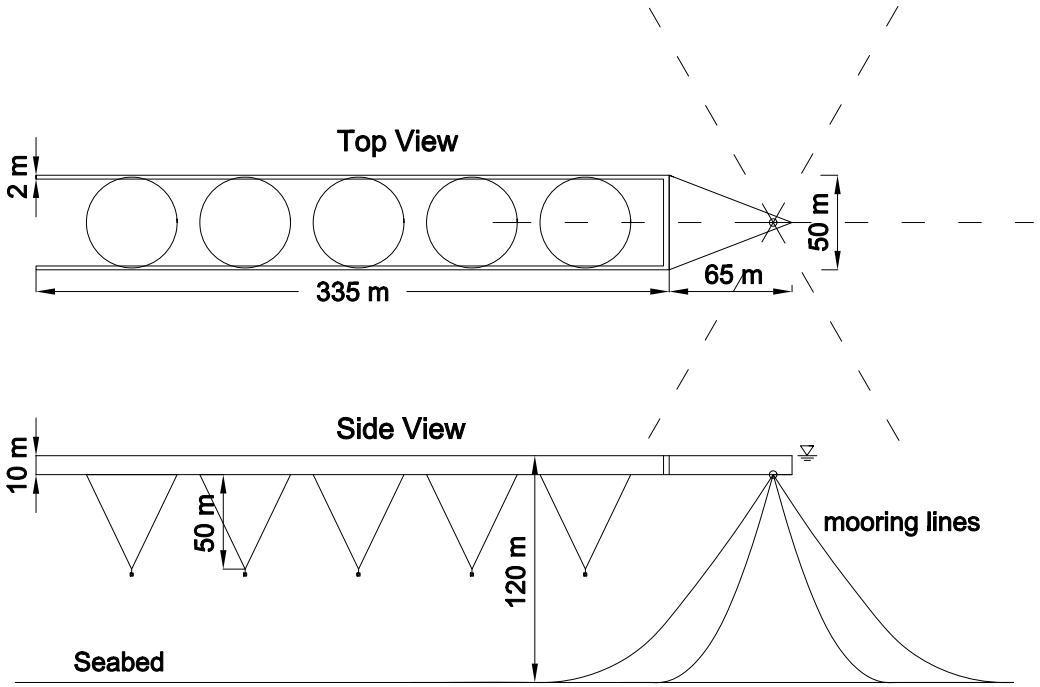

Figure 2: Main geometry of the submerged part of the vessel-shaped fish farm.

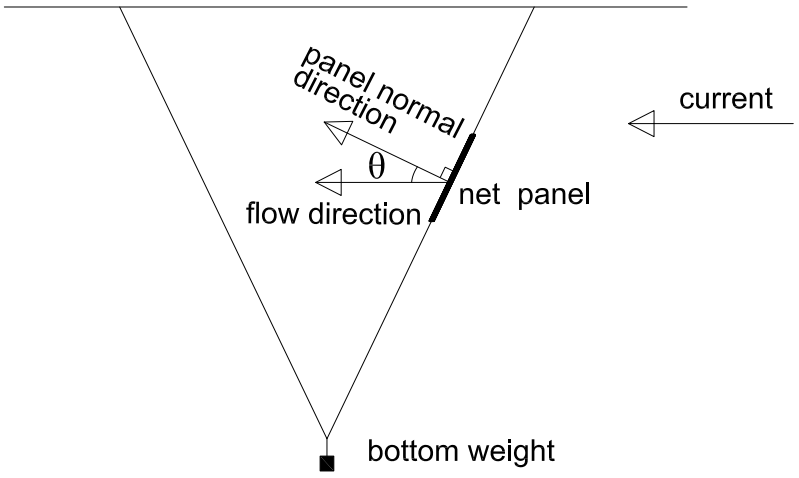

Figure 3: Definition of the angle of attack of a net panel under a steady current.

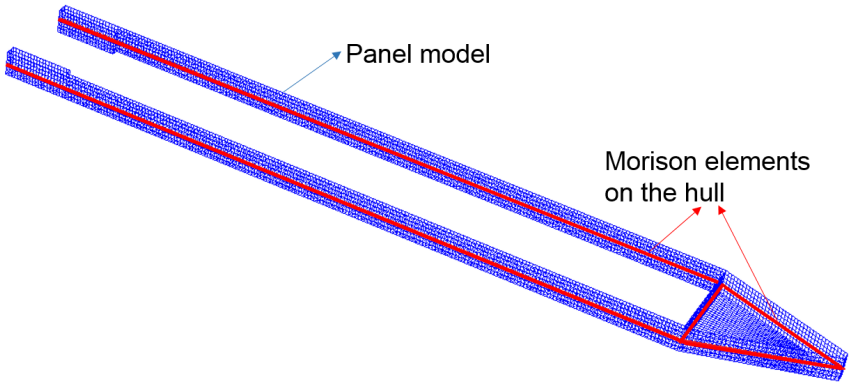

(a)

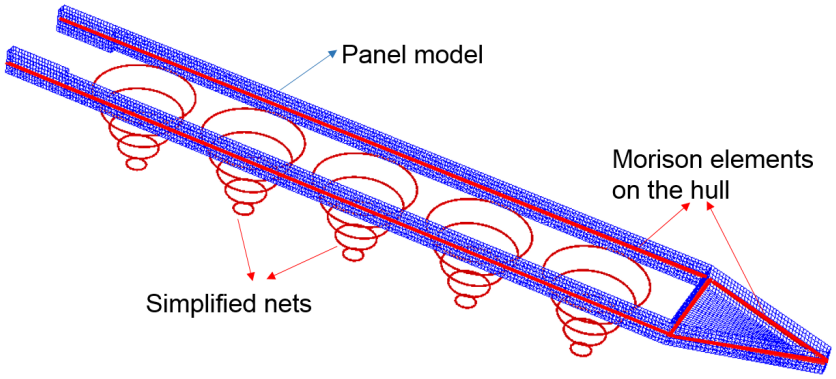

(b)

Figure 4: Illustration of Models 2 and 4 for hydrodynamic analysis in WADAM. (a) M2 panel model with Morison elements on the hull; (b) M4 panel model with Morison elements on the hull and the simplified nets.

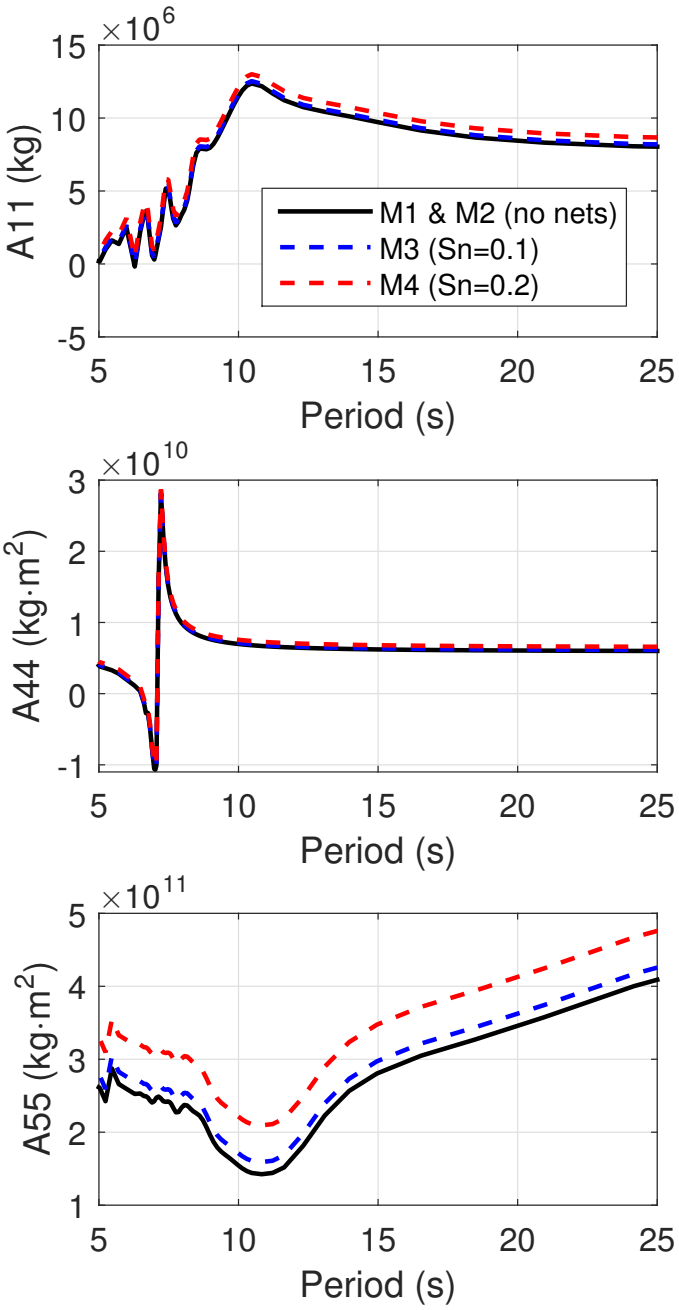

Figure 5: Comparison of the added masses using different models.

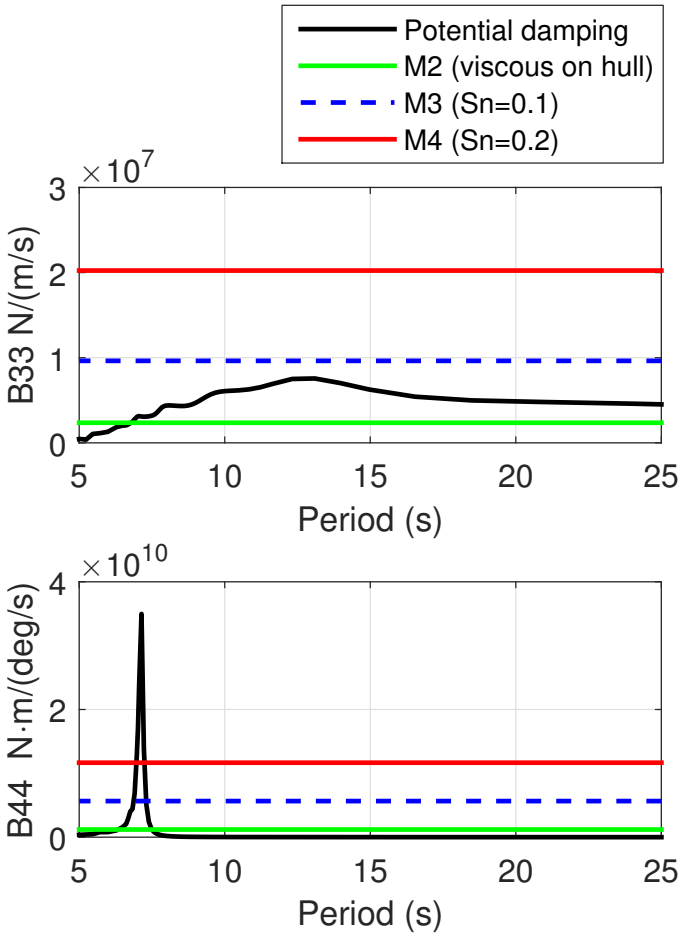

Figure 6: Comparison of potential damping from Model 1 and linearized drag damping from Models 2 to 4.

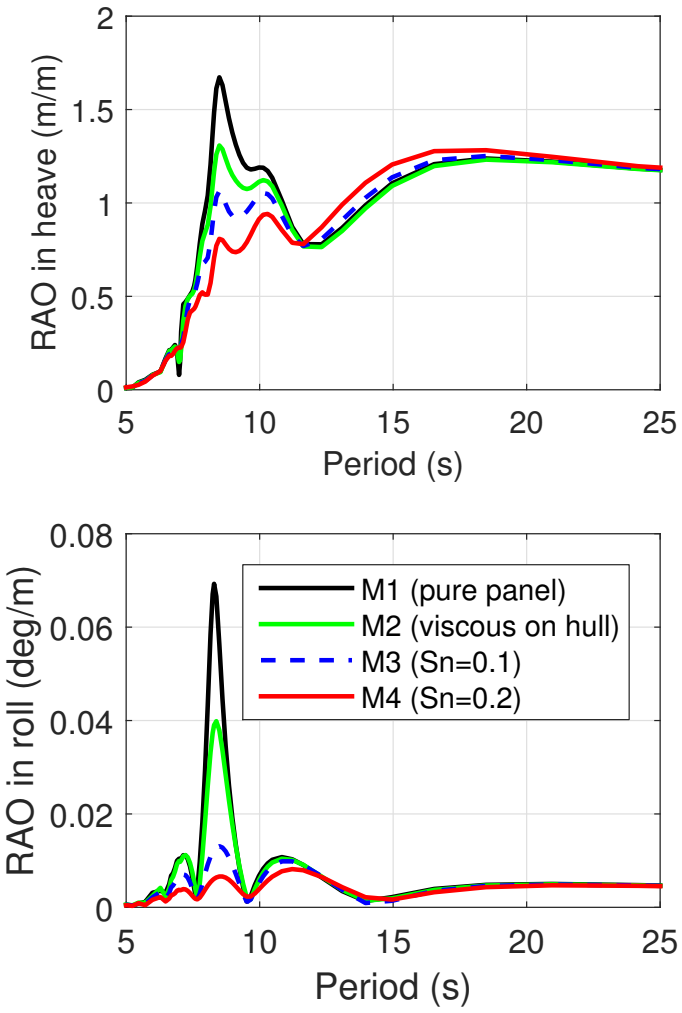

Figure 7: Comparison of RAO in heave and roll from Models 1 to 4 (wave direction = 135 degrees).

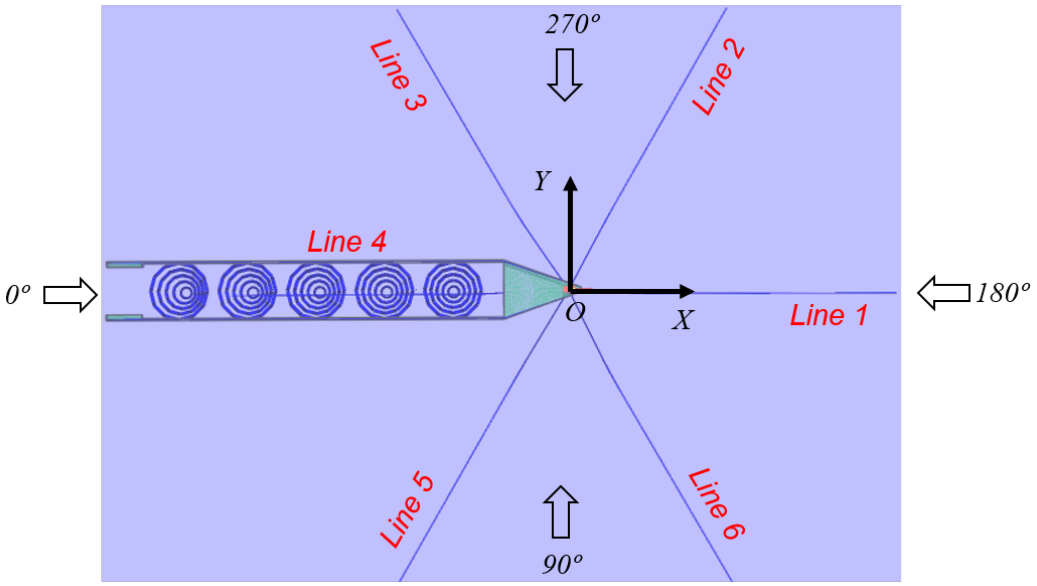

Figure 8: Illustration of coupled model (Model 4) in SIMO-Riflex for time-domain analysis with global coordinate system and mooring line numbers.

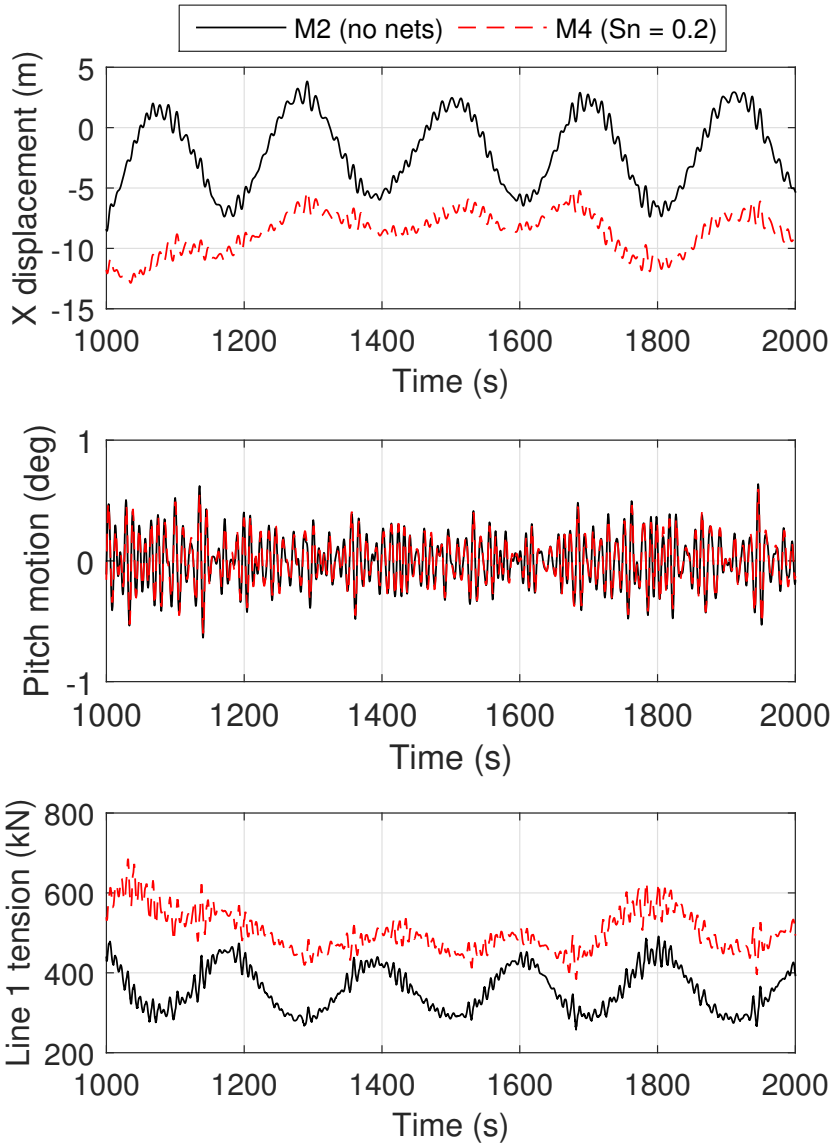

Figure 9: Selected response time histories under EC4 using Models 2 and 4.

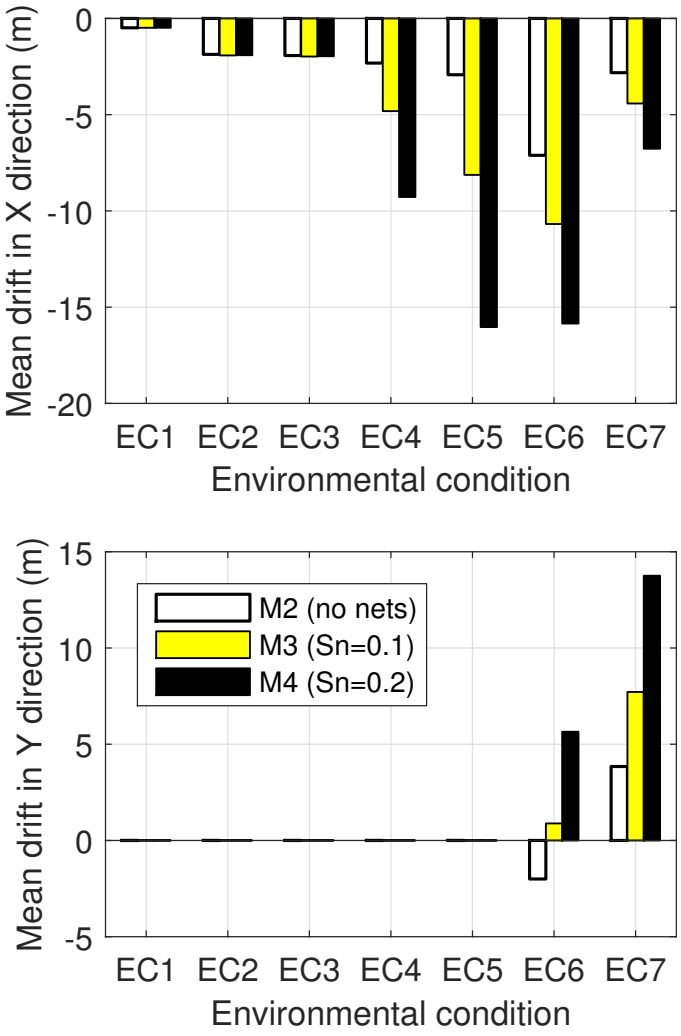

Figure 10: Comparison of mean drift motions of the global origin (turret centre) under all ECs using three models.

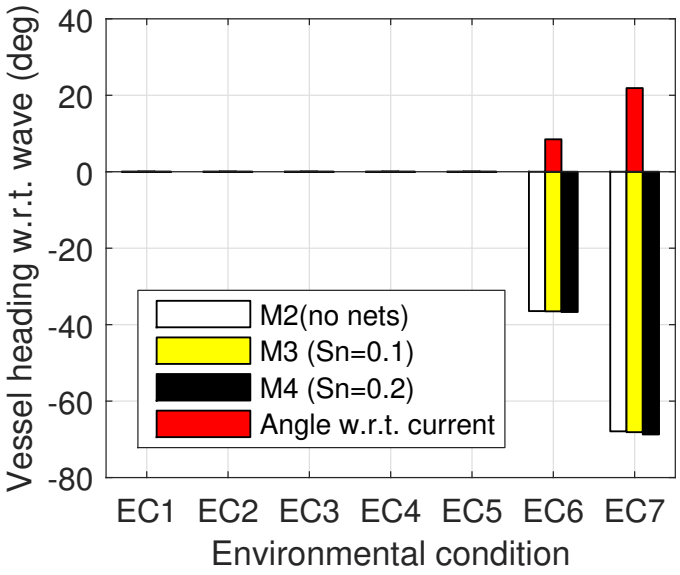

Figure 11: Mean angle difference between the vessel heading and the directions of waves and currents under all ECs.

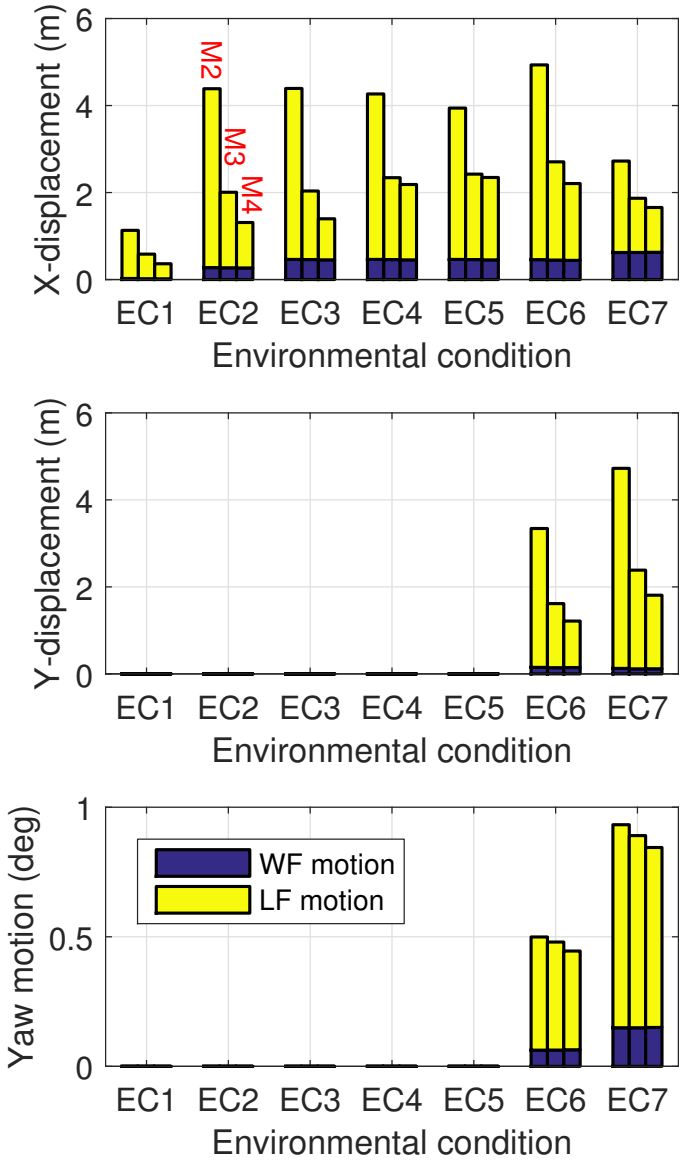

Figure 12: Standard deviations of WF and LF components for horizontal motions using three models (for each EC, from left to right the bars correspond to M2, M3 and M4).

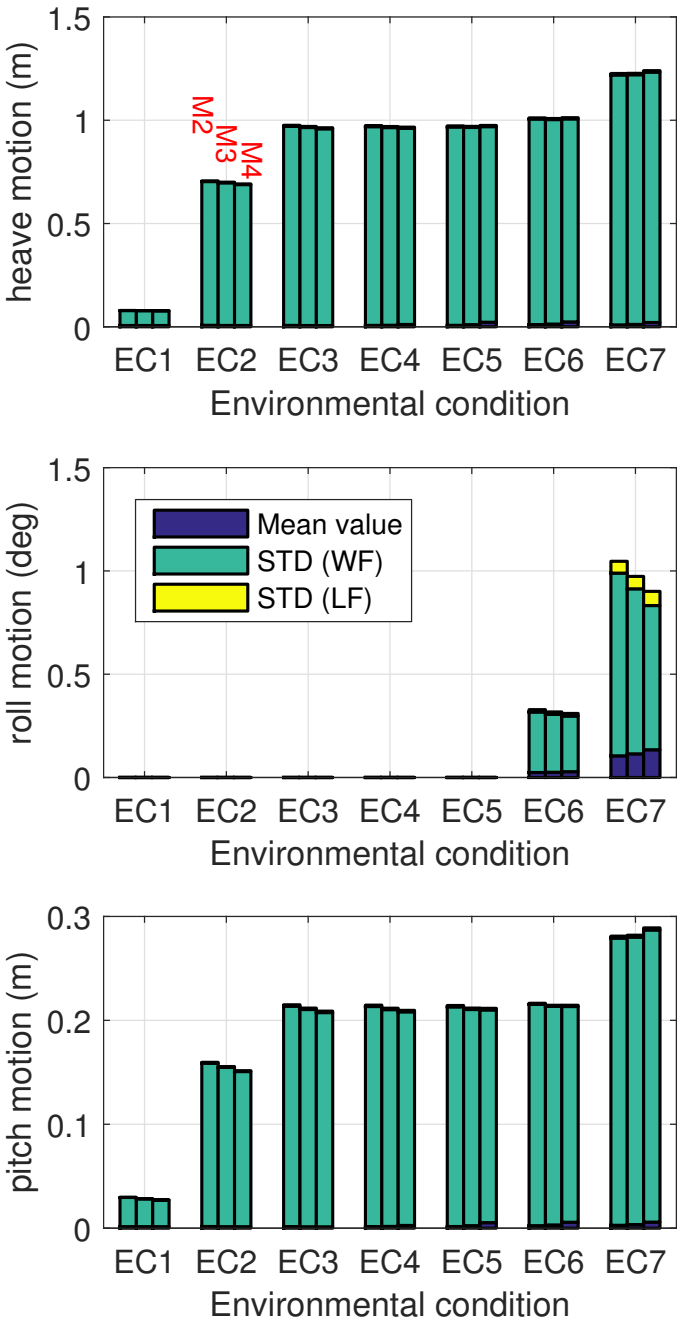

Figure 13: Comparison of mean, WF and LF components from vertical motions using three models (for each EC, from left to right the three bars corresponds to M2, M3 and M4).

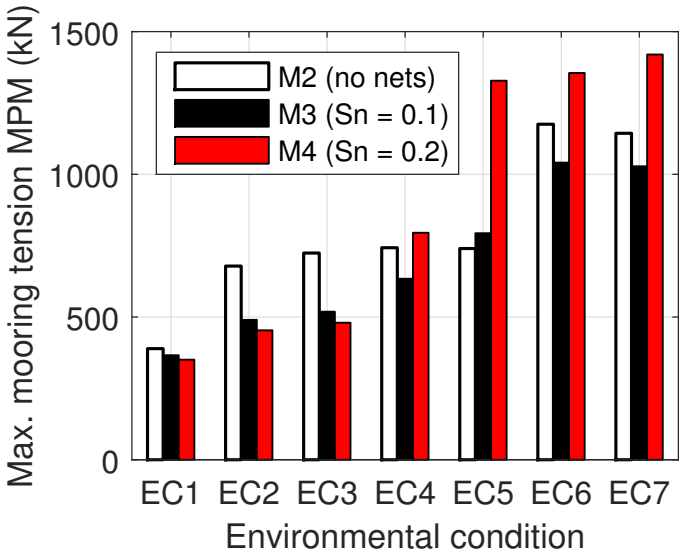

Figure 14: Comparison of maximum tension MPM among six mooring lines (Models 2 to 4, ECs 1 to 7).

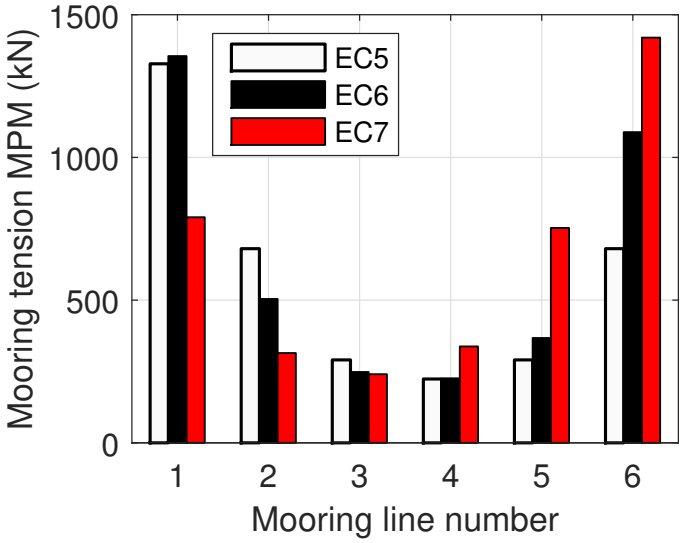

Figure 15: Comparison of the tension MPMs under different ECs (Numerical Model 4).

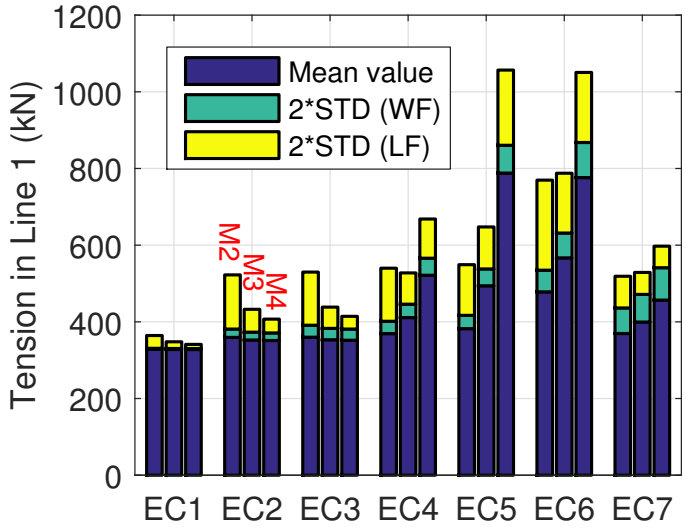

Figure 16: Comparison of mean, WF and LF components for tensions in mooring line 1 using three models (for each EC, from left to right the three bars corresponds to M2, M3 and M4).

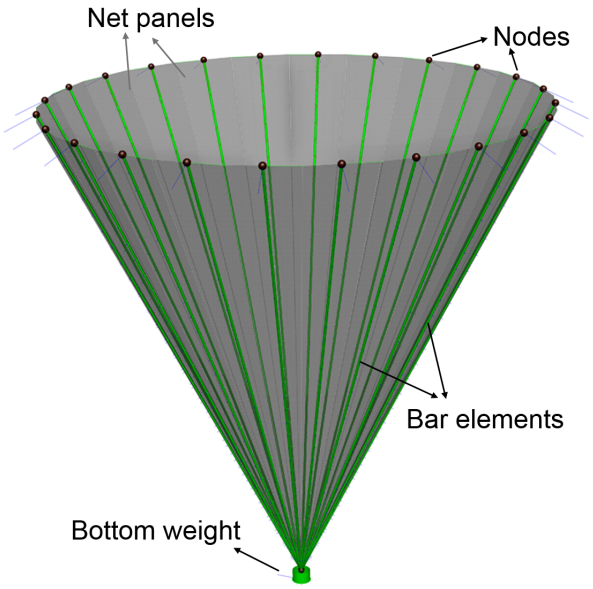

Figure 17: The flexible fish net model using representative bar elements.

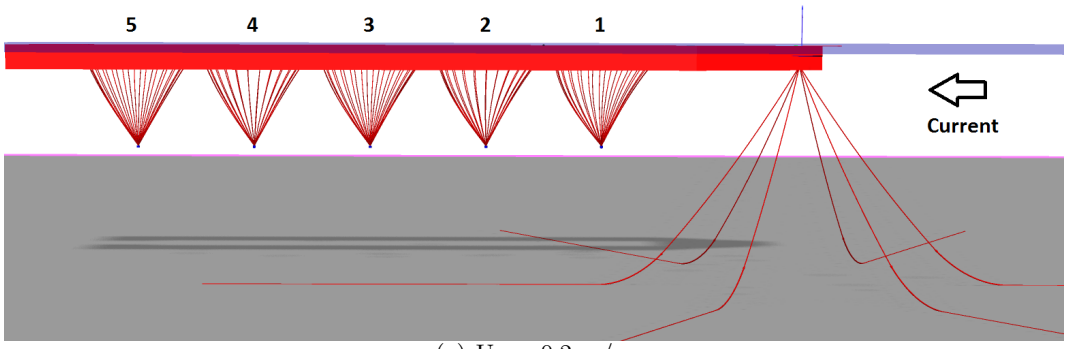

(a) Uc = 0.2 m/s

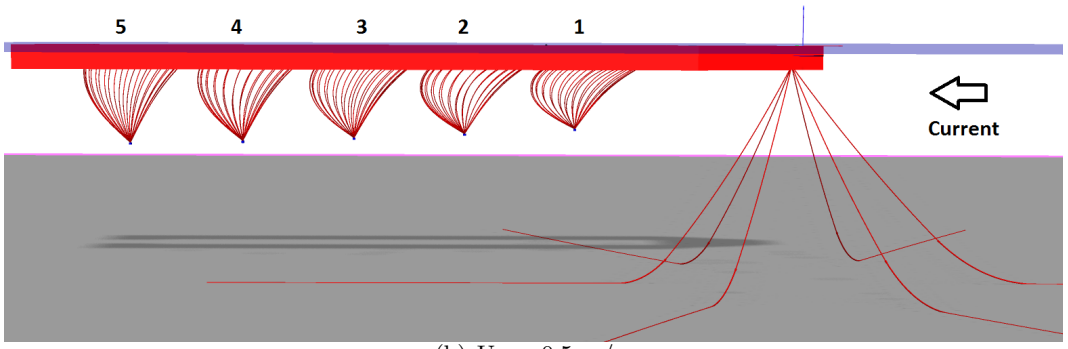

(b) Uc = 0.5 m/s

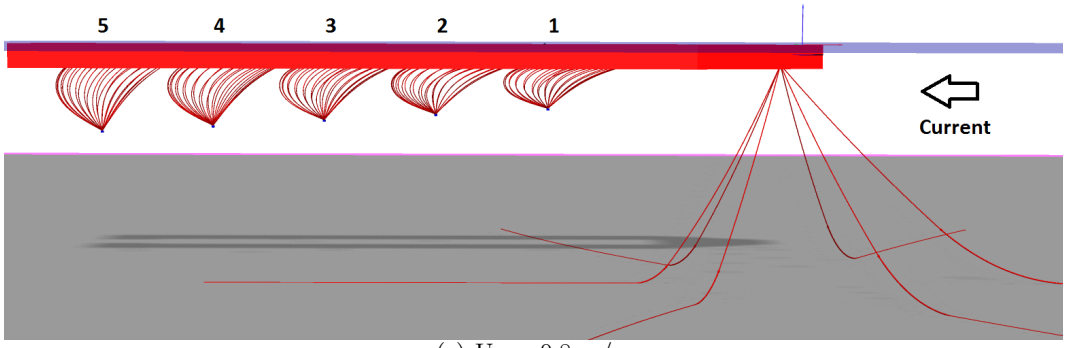

(c) Uc = 0.8 m/s

Figure 18: Illustration of the deformation of flexible nets in steady currents.

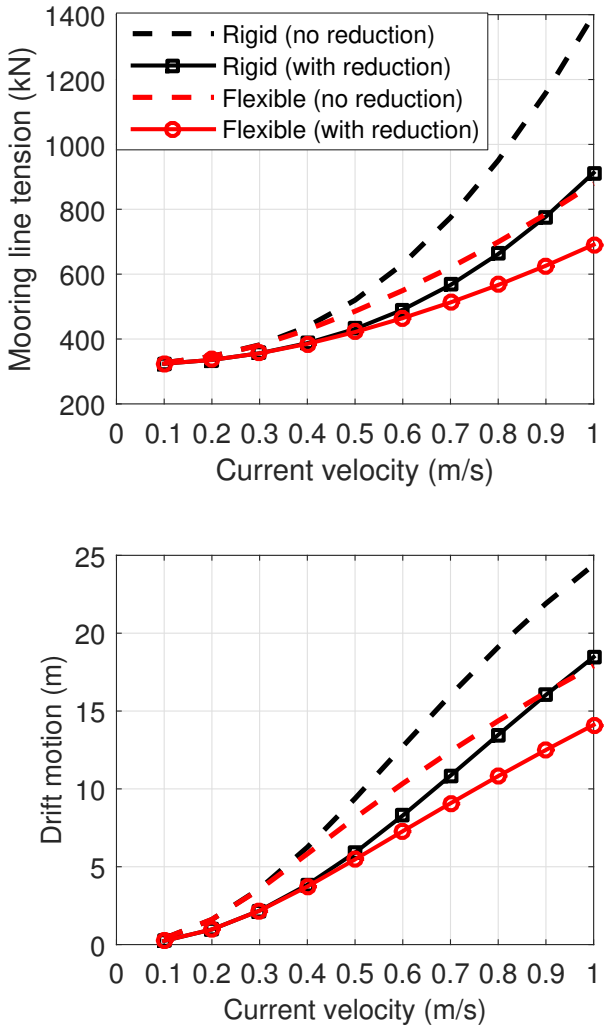

Figure 19: Mooring line tension and drift motion of the turret centre using rigid and flexible net models.